On the Application of the Wiener–Hopf Technique to Electrostatic Field Problems in Interdigital Transducers

Andreas F. Molisch, *Student Member, IEEE,* Ali R. Baghai-Wadji, *Member, IEEE* and Christian O. Schiebl

***Abstract*—Using the Wiener–Hopf-technique, we compute the electrostatic field distribution of interdigital transducers at the plane interface of two dielectric media sandwiched between two grounded metallic plates and neighbored by two grounded semi-infinite plates at the interface. To this end, we compute, for the first time, the associated Green's function, which already satisfies the boundary conditions at all the grounded plates. Consecutively, the Green's function is used to derive the elements of the charge-potential-interrelation matrix for various basis- and testing functions for a method-of-moments application. Examples demonstrate that the new method has considerable advantages with respect to accuracy and computer-memory requirements.**

I. Introduction

The WIENER-HOPF-TECHNIQUE (WHT) is a method for treating boundary-value problems involving semi-infinite structures [1]–[3]. It has already been applied successfully to various electromagnetic [4]–[7] and acoustic scattering problems [8], [9] and some selected eigenvalue problems [10] but, to our knowledge, not to electrostatic problems involving semi-infinite plates together with multiple disconnected metallic bodies.

Surface acoustic wave (SAW) filters are widespread for signal processing applications in the frequency range from 30 MHz to a few GHz. SAWs are excited by applying an alternating electric voltage to the electrodes of an interdigital transducer (IDT). The frequency response of these devices is directly related to the Fourier transform of the corresponding charge distribution underneath the electrodes of the IDT, because the charge can be regarded as the source of the excitation of acoustic waves [11]. Due to the significant difference between electromagnetic and acoustic wave propagation velocities, simulations based on the electrostatic charge distribution give excellent results up to several GHz [11], [12]. Thus the computation of the electrostatic charge distribution becomes of prime importance in the precise modeling and simulation of SAW devices [13]. In these devices there often exist metallic structures that can be modeled as semi-infinite elements [14]. The main objective of the present paper is to show that the WHT can be combined efficiently with numerical techniques to deal simultaneously with the semi-infinite elements and the usual finite metallic structures, thus avoiding the considerable numerical problems that are usually associated with semi-infinite structures.

The geometry of our problem is sketched in Fig. 1(a). It was shown previously [15] that the boundary conditions at $y = \pm b$ can be transformed into the "active" plane $y = 0$, so one possible approach would involve the application of the Method of Moments (MoM) [16]: calculate the Green's function as the potential response to a line charge source (LCS) in the metallic package (excluding the semi-infinite plates); discretize all metallic regions in the active plane and apply the MoM. We will refer to this approach as the direct MoM. Our new approach is: first calculate the Green's function satisfying the boundary conditions of the infinite as well as of the semi-infinite plates; then discretize only the electrodes in the active middle zone $-a < x < a, y = 0$; and finally apply the MoM. We will call this technique the WH-MoM (Wiener–Hopf MoM). As shown below, it has considerable advantages with respect to accuracy and computer-memory requirements.

Thus the objectives of this work are twofold: from a theoretical point of view, for the first time we derive the aforementioned Green's function and prove that it is possible to transform the boundary conditions of *all* the metallic plates into an active middle zone. From a practical point of view, we provide a powerful mathematical tool to tackle boundary-value problems in connection with SAW devices.

II. Theory

A. Formulation of the Problem

In order to calculate the Green's function, we use Jones' version of the WHT, [2], [3], [17], [18]. The 2-D-geometry is shown in Fig. 1(b): a LCS of unit strength is located at $x = x_1$. The substrate is assumed to be isotropic (for a discussion of this assumption, see Section II-D). For the time being, a harmonic time-dependence for the LCS with an angular frequency ω is assumed, where ω is small enough for quasielectrostatic calculations to be valid. In the following, the

Manuscript received July 25, 1991; revised June 1, 1992.

A. F. Molisch was with the Institut für Allgemeine Elektrotechnik und Elektronik, Technische Universität Wien, Gußhausstraße 27–29, A-1040 Vienna Austria. He is presently with the Institut für Nachrichtentechnik und Hochfrequenztechnik, Technische Universität Wien, Gußhausstraße 25, 1040 Vienna, Austria.

A. R. Baghai-Wadji is with the Institut für Allgemeine Elektrotechnik und Elektronik, Technische Universität Wien, Gußhausstraße 27–29, A-1040 Vienna, Austria.

C. O. Schiebl is with Digital Equipment Corporation, Campusbased Engineering Center, Favoritenstrabe 7, A-1040 Vienna, Austria.

IEEE Log Number 9204493.

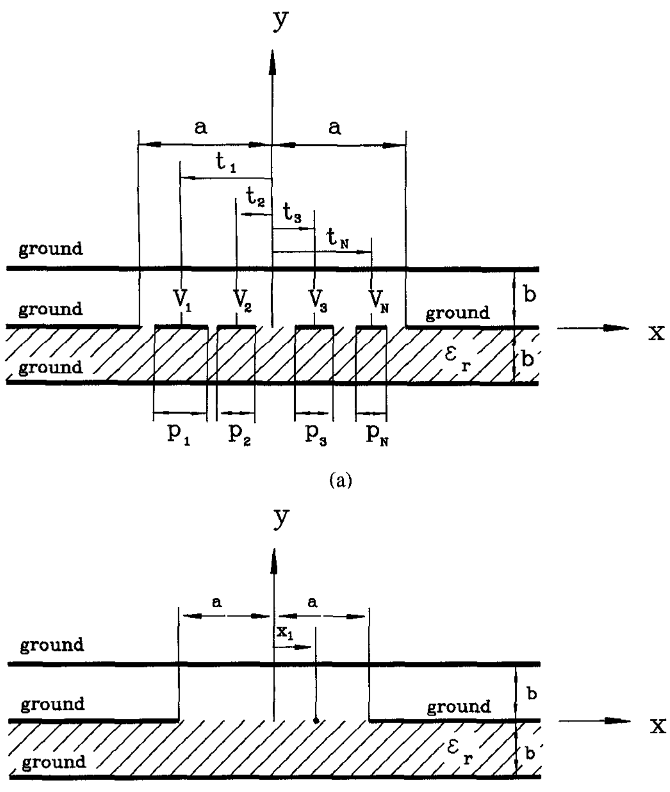

Fig. 1. (a) General geometry of a shielded IDT with semi-infinite plates and N electrodes. (b) Geometry for the computation of the Green's function.

factor exp $(j\omega t)$ is omitted. The dielectric is assumed to have a permittivity with Im $\{\epsilon\} > 0$. The Fourier transform of the Helmholtz equation for the scalar potential ϕ, satisfying the Sommerfeld radiation condition, is

$$\frac{d^2\overline{\phi}(\alpha,y)}{dy^2} - \gamma^2\overline{\phi}(\alpha,y) = 0,$$
$$\gamma^2 = \alpha^2 - \omega^2\epsilon\mu = \alpha^2 - k^2, \tag{1}$$

where the bar denotes Fourier transform (FT). Let us now define

$$\overline{\rho}_+(\alpha) = \int_a^{+\infty} \rho(x,0)e^{j\alpha(x-a)}dx, \tag{2}$$
$$\overline{\phi}_1(\alpha) = \int_{-a}^{a} \phi(x,0^+)e^{j\alpha x}dx, \tag{3}$$
$$\overline{\rho}_-(\alpha) = \int_{-\infty}^{-a} \rho(x,0)e^{j\alpha(x+a)}dx. \tag{4}$$

The subscripts + and −, respectively, signify regularity in upper ($\tau > -k_2 = \tau_-$) and lower ($\tau < k_2 = \tau_+$) half-planes of the complex plane $\alpha = \sigma + j\tau$, where $k_2 = \text{Im}\{k\} > 0$. The assumption of a finite ω makes sure that the half-planes overlap.

At the interface, $D_y(x,0^+) - D_y(x,0^-) = \rho(x,0)$. Here, D_y denotes the y-component of the electric displacement. The x-component of the electric field E_x is continuous in the middle zone of the interface and zero at the semiinfinite and infinite plates. Imposing these conditions, charge and potential satisfy the following equation [19]

$$e^{j\alpha a}\overline{\rho}_+(\alpha) - \epsilon_0(1+\epsilon_r)\gamma\coth(\gamma b)\overline{\phi}_1(\alpha) + e^{-j\alpha a}\overline{\rho}_-(\alpha) = -\overline{s}_1(\alpha) + \omega\overline{F}_s(\alpha), \tag{5}$$

where $\overline{s}_1(\alpha) = \exp(j\alpha x_1)$ is the FT of the LCS located at x_1. The term $\omega\overline{F}_s(\alpha)$ stands for the contribution of the solenoidal vector potential. As we mentioned above, we wish to consider the quasielectrostatic case so that this term can be omitted henceforth.

B. Solution of the Three-part Wiener–Hopf Equation

The function $b\gamma\coth(\gamma b) = \overline{K}(\alpha)$ can be factorized into $\overline{K}_+(\alpha)\cdot\overline{K}_-(\alpha)$, where $\overline{K}_+(\alpha)$ and $\overline{K}_-(\alpha)$ are regular and nonzero in the half-plane $\tau > \tau_-$ and $\tau < \tau_+$, respectively. $\overline{K}(\alpha)$ is regular in the strip $-k_2 < \tau < k_2$ and the relation $\overline{K}_+(\alpha) = \overline{K}_-(-\alpha)$ holds. Multiplying (5) by $\exp(-j\alpha a)/\overline{K}_+(\alpha)$ and invoking the decomposition theorem [3, p. 13], we obtain

$$\frac{\overline{\rho}_+(\alpha)}{\overline{K}_+(\alpha)} + \frac{1}{2\pi j}\int_{-\infty+jc}^{\infty+jc}\frac{\overline{\rho}_-(\xi)e^{-2j\xi a}}{(\xi-\alpha)\overline{K}_+(\xi)}d\xi + \frac{1}{2\pi j}\int_{-\infty+jc}^{\infty+jc}\frac{\overline{s}_1(\xi)e^{-j\xi a}}{(\xi-\alpha)\overline{K}_+(\xi)}d\xi$$
$$= \frac{1}{2\pi j}\int_{-\infty+jd}^{\infty+jd}\frac{\overline{\rho}_-(\xi)e^{-2j\xi a}}{(\xi-\alpha)\overline{K}_+(\xi)}d\xi + \frac{1}{2\pi j}\int_{-\infty+jd}^{\infty+jd}\frac{\overline{s}_1(\xi)e^{-j\xi a}}{(\xi-\alpha)\overline{K}_+(\xi)}d\xi + \epsilon_0\frac{1+\epsilon_r}{b}e^{-j\alpha a}\overline{K}_-(\alpha)\overline{\phi}_1(\alpha) = \overline{I}(\alpha). \tag{6}$$

The leftmost side of (6) is regular and bounded in the upper half-plane, while the middle term is regular and bounded in the lower half-plane. Combining the edge-conditions (charge near the edge $x \to 0$ of a metallic plate goes to infinity like $x^{-\eta}$, where $0 < \eta < 1$, [20]) with the Abelian theorem [3, p. 36], we see that $\overline{I}(\alpha)$ tends to zero in the limit $\alpha \to \infty$. Thus, by Liouville's theorem [21, p. 381], we obtain $\overline{I}(\alpha) \equiv 0$. It turns out that we only need the equation which arises by setting the leftmost side of (6) equal to zero. Multiplying (5) by $\exp(j\alpha a)/\overline{K}_-(\alpha)$, and proceeding analogously, we obtain a similar integral equation. These two equations can be decoupled by introducing the functions

$$\overline{\psi}_i(\alpha) = \overline{\rho}_+(\alpha) + (-1)^{i+1}\overline{\rho}_-(-\alpha), \qquad i = 1,2. \tag{7}$$

At this point, we go to the limit $\omega \to 0$ to come back to our initial electrostatic problem (the operations performed on (5) and the limiting process $\omega \to 0$ are interchangeable). We then evaluate the occuring integrals using the residue theorem to get

$$\frac{\overline{\psi}_i(\alpha)}{\overline{K}_+(\alpha)} + (-1)^i\sum_{n=1}^{\infty}\frac{\overline{\psi}_i(\alpha_n)e^{2j\alpha_n a}}{(\alpha_n+\alpha)}\cdot\text{Res}\left\{\frac{1}{\overline{K}_-(\alpha)}\right\}\Bigg|_{\alpha=\alpha_n}$$
$$= \sum_{n=1}^{\infty}\frac{[\overline{s}_1(-\alpha_n) - (-1)^i\overline{s}_1(\alpha_n)]e^{j\alpha_n a}}{(\alpha_n+\alpha)}\cdot\text{Res}\left\{\frac{1}{\overline{K}_-(\alpha)}\right\}\Bigg|_{\alpha=\alpha_n}, \tag{8}$$

where the α_n denote the poles of $\overline{K}_-(\alpha)$ in the upper complex half-plane. In the electrostatic limit, the function $\overline{K}(\alpha)$ becomes $\overline{K}(\alpha) = b\alpha \coth(\alpha b)$, with

$$\overline{K}_+(\alpha) = \sqrt{\pi}\frac{\Gamma(1 - j\alpha b/\pi)}{\Gamma(1/2 - j\alpha b/\pi)};$$
$$\alpha_n = j\left(n - \frac{1}{2}\right)\frac{\pi}{b}, \tag{9}$$

$$\operatorname{Res}\left\{\frac{1}{\overline{K}_-(\alpha)}\right\}\Bigg|_{\alpha=\alpha_n} = p_n = \frac{-j}{b}\cdot\frac{1\cdot 3\cdot\cdots\cdot(2n-3)}{2\cdot 4\cdot\cdots\cdot(2n-2)}, \tag{10}$$

where p_1 by definition equals $-j/b$ and Γ is the complex Gamma function as defined by [22]. Setting $\alpha = \alpha_k$ in (8), we get an infinite system of complex algebraic equations for the unknowns $\overline{\psi}_i(\alpha_n)$. However, the terms of the series decay as $\exp(-2n\pi a/b)$ and $\exp[-n\pi(a - |x_1|)/b]$, respectively (note that a is larger than $|x_1|$) and thus in most cases we get sufficiently accurate results by truncating the sum after, say, 10 to 20 terms.

C. The Green's Function

After solving the above system of equations, we use (8) and (7) to obtain in the wavenumber domain an expression for the charge distribution in the active plane

$$\overline{\rho}(\alpha|x_1) = \overline{s}_1(\alpha) + \overline{\rho}_+(\alpha) + \overline{\rho}_-(\alpha), \tag{11}$$

where

$$\overline{\rho}_+(\alpha) = e^{j\alpha a}\overline{K}_+(\alpha)\cdot\sum_{n=1}^{\infty} p_n\frac{1}{(\alpha+\alpha_n)}\cdot\left[\frac{1}{2}(\overline{\psi}_{1n} - \overline{\psi}_{2n})e^{2j\alpha_n a} + \overline{s}_1(-\alpha_n)e^{j\alpha_n a}\right]$$
$$\overline{\rho}_-(\alpha) = e^{-j\alpha a}\overline{K}_+(-\alpha)\cdot\sum_{n=1}^{\infty} p_n\frac{1}{(-\alpha+\alpha_n)}\cdot\left[\frac{1}{2}(\overline{\psi}_{1n} + \overline{\psi}_{2n})e^{2j\alpha_n a} + \overline{s}_1(\alpha_n)e^{j\alpha_n a}\right],$$

where $\overline{\psi}_{1n}$ and $\overline{\psi}_{2n}$ stand for $\overline{\psi}_1(\alpha_n)$ and $\overline{\psi}_2(\alpha_n)$, respectively. Inverse Fourier transform then gives $\rho(x|x_1)$.

In (11), it can be seen that $\overline{\rho}_+(\alpha)$ consists of charges induced by the line charge (the terms involving $\overline{s}_1$) and by the charges on the left plate. $\overline{\rho}_-(\alpha)$ can be interpreted analogously. The edge behavior was checked by means of the Abelian theorem: $\rho(x|x_1)$ asymptotically behaves like $(|x| - a)^{-1/2}$ in the limit $|x| - a \to 0^+$.

The potential in the active plane is related to the charge distribution by (5) in the limit $\omega\overline{F}_s \to 0$. With this result, the potential due to an LCS at $x = x_1$ is uniquely determined for all α and y. Inverse Fourier transform gives

$$\phi(x,y) = \frac{1}{2\pi\epsilon_0(1+\epsilon_r)}\int_{-\infty}^{\infty}\overline{\rho}(\alpha|x_1)\frac{\sinh[\alpha(b-|y|)]}{\alpha\cosh(\alpha b)}e^{-j\alpha x}d\alpha, \tag{12}$$

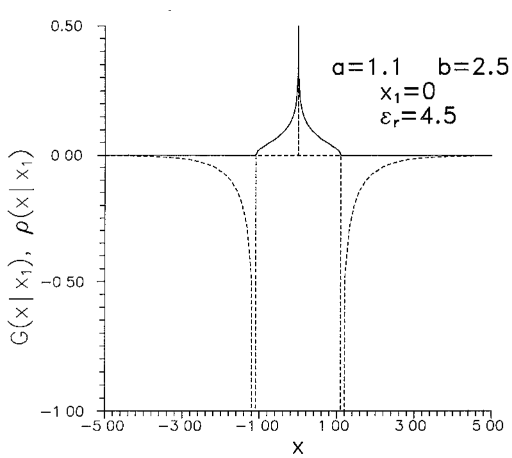

Fig. 2. Green's function (solid) and charge density distribution (dashed) due to a line charge source located at $x_1 = 0$. The parameters a, b, x_1 and ϵ_r refer to the geometry in Fig. 1(b). x, x_1, a, and b are in units of $L = 200\,\mu$m. $\rho(x|x_1)$ is in $4.427\cdot 10^{-8}$ Coulomb/meter (i.e. normalized by ϵ_0/L) and $G(x|x_1) = \phi(x, 0)$ is in volts.

providing a complete description of the field. Now we define the Green's function $G(x|x_1)$ appropriate for our problem as the potential in the plane $y = 0$. Fig. 2 shows the Green's function and the induced charge distribution due to a LCS. It is obvious that for *any* electrode configuration, the knowledge of the charge distribution in the middle zone $\rho_m(x)$ is sufficient to compute the potential $\phi(x,0) = \int G(x|x')\cdot\rho_m(x')dx'$. This proves that the transformation of all boundary conditions into the middle zone is possible. For completeness, in Appendix B we outline the derivation of $\overline{\rho}(\alpha|x_1)$ for the case that only one semi-infinite plate exists.

D. Discussion of Underlying Assumptions

Now let us discuss our assumption of the isotropic substrate. Generally, the substrate materials used in SAW devices are anisotropic. It is well-known that the equation for the electrostatic potential in an anisotropic substrate can be transformed to canonical form (Laplace equation). This involves the coordinate transformation $\hat{x} = x - (\epsilon_{12}/\epsilon_{22})y$ and $\hat{y} = (\epsilon_T/\epsilon_{22})y$, where $\epsilon_T = (\epsilon_{11}\epsilon_{22} - \epsilon_{12}^2)^{1/2}$, [23]. For the calculation of the charge distribution, the only effect of the transformation is that the effective distance of the lower ground plate from the interface becomes scaled by ϵ_T/ϵ_{22}. For the case that $b^u \approx b^d\epsilon_T/\epsilon_{22}$ the above closed-form results remain applicable (b^u and b^d are the distances between the interface and the upper and lower shielding plates, respectively). If this is not the case, the evaluation of the Green's function becomes extremely complicated as the function $\alpha[\coth(\alpha b^u) + \epsilon_T\coth(\alpha b^d\epsilon_T/\epsilon_{22})]$ has to be factorized, which can only be managed numerically. As the usual packaging geometries agree quite well with the above condition and the dependence of the charge distribution on the packaging is very small anyway, our calculations remain valid in most of the practical cases.

The assumption that the semi-infinite plates are located symmetrically with respect to the y-axis implies no loss of generality, because the coordinate system can be chosen accordingly and the location of the electrodes in the middle is arbitrary.

E. The Method of Moments

Given the potentials on the electrodes, the associated charge distribution is to be determined. To compute $\rho(x)$, we apply the MoM [15], [16]. The charge distribution in the active middle zone is approximated by a sum of basis functions $b_l(x)$ which are weighted by unknown coefficients q_l. The testing functions are denoted as $w_k(x)$. The q_l are then computed from

$$\phi_k = \sum q_l A_{kl}, \tag{13}$$

where the matrix A is the charge-potential-interrelation matrix and $\phi_k = \int \phi(x,0) w_k(x)\, dx / \int w_k(x)\, dx$. The detailed expressions for the A_{kl}, selecting various basis- and testing functions, are summarized in Appendix A.

III. Results

For a WH-MoM calculation of the charge distribution in a two-electrode transducer we discretize each of the electrodes into 10 stripes (for the geometry data refer to Fig. 3). Pulse functions are used for both basis- and testing functions. To check the accuracy of other commonly used methods, we compare our present results to those obtained by (i) direct MoM and (ii) Finite Element Method (FEM). Due to the fact that our formalism correctly accounts for the singularities of the charge distribution near the edges of the semi-infinite plates, we expect that the differences in the results will occur mainly in these regions. To make these differences easier to inspect, we compare the results in the wavenumber domain rather than in the spatial domain, transforming the differences into the higher wavenumber range. Fig. 3 compares the direct MoM to the WH-MoM. Applying direct MoM, we discretize each electrode into 10 strips; the semi-infinite plates are truncated at $|x| = 9.7$ and discretized into 80 strips each. We see that the direct MoM gives quite accurate results for $\alpha < 4\pi$ (difference between the two methods is smaller than 0.52 for $\alpha < 2\pi$ and smaller than 1.4 for $2\pi < \alpha < 4\pi$ where the maximum values of $\overline{\rho}(\alpha)$ in these regions are 37.3 and 12.9, respectively; α and $\overline{\rho}(\alpha)$ are normalized according to Fig. 3). At larger wavenumbers the difference can become quite significant. Fig. 4 shows a comparison between FEM [24] and WH-MoM. The simulation range is the domain $|x| < 9.7, |y| < b$. As the FEM program is not able to deal with infinite elements, the structure was made periodic in the x-direction, which is equivalent to imposing homogeneous Neumann boundary conditions at $|x| = 9.7, |y| < b$. An automatic grid generator adapts the grid for consecutive computation cycles until the relative difference between the total energies from two subsequent cycles becomes smaller than 1%. The presented results are achieved with a total number of 104 elements in x-direction. The absolute difference of $\overline{\rho}(\alpha)$ computed by FEM and WH-MoM is smaller than 2.2 for $\alpha < 2\pi$ and smaller than 3.2 for $2\pi < \alpha < 4\pi$.

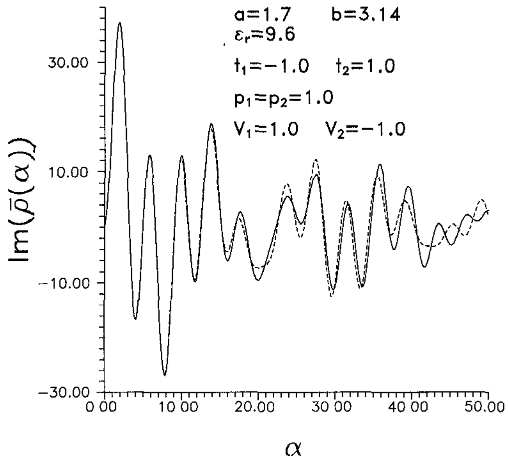

Fig. 3. Imaginary part of the Fourier transform of the charge density distribution on a two-electrode IDT with semi-infinite plates (real part is zero): this work (solid) and direct MoM [15] (dashed). The parameters a, b, t_1, t_2, p_1, p_2 are all measured in units of $L = 100\,\mu$m; parameters V_1 and V_2 are measured in volts. All parameters refer to Fig. 1(a). The wavenumber α is in units of $1/L$. The units on the ordinate-axis are $8.854 \cdot 10^{-12}$ Coulomb (i.e. normalized by ϵ_0).

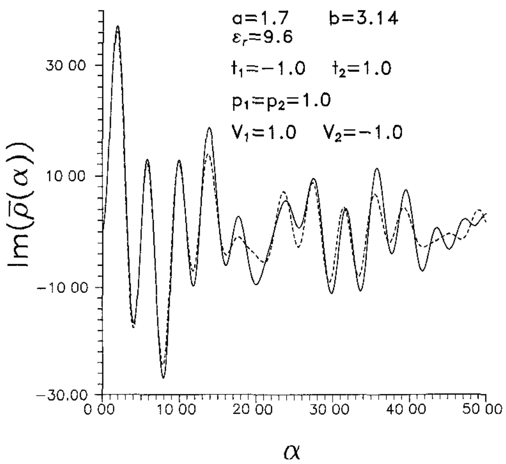

Fig. 4. Imaginary part of the Fourier transform of the charge density distribution on the two-electrode IDT from Fig. 3 (real part is zero): this work (solid) and FEM [24] (dashed), geometry data and normalization as in Fig. 3.

Our second example presents the results for a five-electrode trasducer (see Fig. 5 for the geometry data and the charge distribution). For both WH-MoM and direct MoM, each electrode was divided into 10 stripes. For the direct MoM, the semi-infinite plates were truncated at $|x| = 12$ and divided into 80 strips each. The absolute difference between the two methods was smaller than 0.5 for $\alpha < 2\pi$, smaller than 0.75 for $2\pi < \alpha < 4\pi$, and smaller 1.2 for $4\pi < \alpha < 6\pi$; the maximum values of $\overline{\rho}(\alpha)$ in these regions are 59.9, 6.0 and 27.9, respectively (normalization according to Fig. 6). The corresponding potential distribution is shown in Fig. 7. Note that the boundary conditions at $|x| > a$ are satisfied exactly.

In calculating the charge-potential-interaction matrix elements, the memory requirements were smaller by a factor 50 for the two-electrode transducer and a factor 8 for the five-electrode transducer compared to direct MoM.

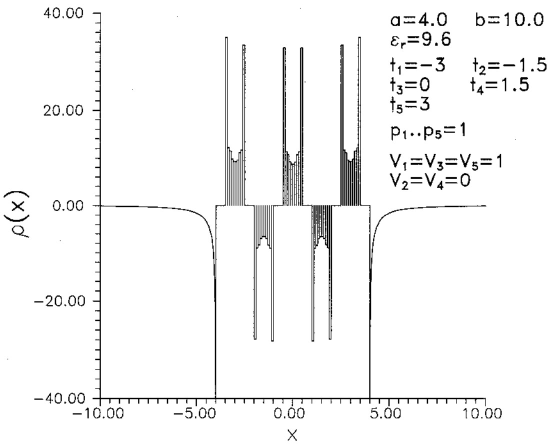

Fig. 5. Charge density distribution on a five-electrode IDT with semi-infinite plates computed by WH-MoM. The parameters $a, b, t_1 \cdots t_5, p_1 \cdots p_5$ are all measured in units of $L = 50\,\mu$m; parameters $V_1 \cdots V_5$ are measured in Volts. All parameters refer to Fig. 1(a). The units on the ordinate axis are $1.7708 \cdot 10^{-7}$ Coulomb/meter (normalized by ϵ_0/L).

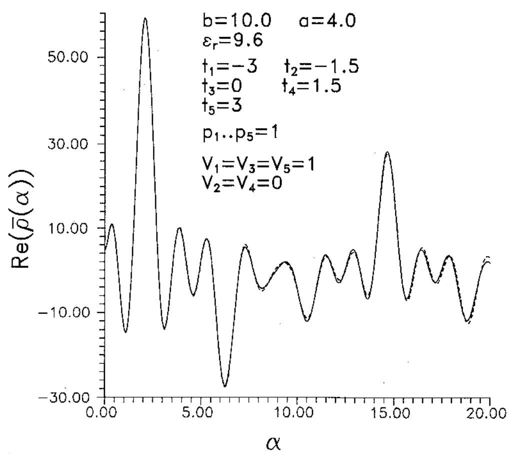

Fig. 6. Real part of the Fourier transform of the charge distribution on the five-electrode IDT from Fig. 5 (imaginary part is zero): this work (solid) and direct MoM (dashed). The geometry and the units of the parameters is the same as in Fig. 5. α is measured in units of $1/L = 1/50\,\mu$m. The units on the ordinate axis are $8.854 \cdot 10^{-12}$ Coulomb (normalized by ϵ_0).

IV. Conclusion

Using the Wiener–Hopf-technique, we computed the electrostatic Green's function of a line charge at the interface of two dielectric media shielded by a metallic package and neighbored by two semi-infinite plates at the interface. We gave a closed-form equation for the Green's function in the Fourier transform domain; and the possibility of transforming all the boundary conditions into the active zone was shown. We then calculated the elements of the charge-potential-interrelation matrix for a MoM-application and compared our results with those obtained by direct Method of Moments and Finite Element Method. Our method has two major advantages: (i) due to the exact representation of the singularities near the edges of the semi-infinite plates, it is more accurate. (ii) as the boundary conditions on the semi-infinite plates are already satisfied, we only have to discretize the active middle zone, so that considerably smaller matrices have to be handled. The method also can be used to extend the capacitance

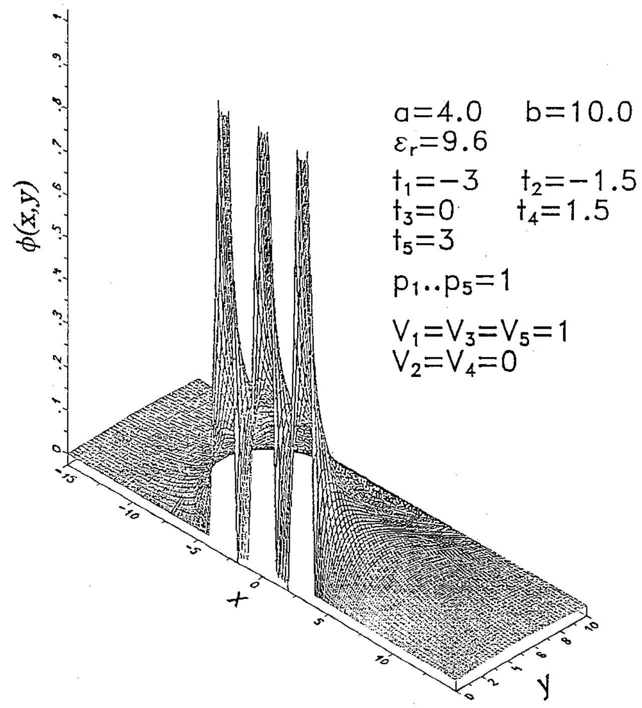

Fig. 7. Potential distribution of the five-electrode IDT from Fig. 5 for the region $y \geq 0$ (symmetrical with respect to the x-axis). The parameters and the normalization are the same as in Fig. 5; the potential $\phi(x, y)$ is measured in volts.

computations by parallel track subdivision of SAW-IDT's [25], [26].

Appendix A

In this appendix, we summarize the MoM equations for various basis- and testing functions. The derivation runs along the lines outlined in Section II. For an arbitrary given charge density distribution $b_l(x)$, with the Fourier transform $\overline{b}_l(\alpha)$, the $\overline{\psi}_{in}$ are computed from

$$\frac{\overline{\psi}_{im}}{\overline{K}_+(\alpha_m)} + (-1)^i \sum_{n=1}^{\infty} \frac{\overline{\psi}_{in} e^{2j\alpha_n a}}{(\alpha_n + \alpha_m)} p_n = \sum_{n=1}^{\infty} \frac{[\overline{b}_l(-\alpha_n) - (-1)^i \overline{b}_l(\alpha_n)] e^{j\alpha_n a}}{(\alpha_n + \alpha_m)} p_n. \quad \text{(A1)}$$

The function $\overline{\rho}(\alpha|x_l)$ is then given by

$$\overline{\rho}(\alpha|x_l) = \overline{b}_l(\alpha) + \overline{\rho}_+(\alpha) + \overline{\rho}_-(\alpha) \quad \text{(A2)}$$

where $\overline{\rho}_+$ and $\overline{\rho}_-$ are given by (11) with $\overline{s}_1$ replaced by $\overline{b}_l$.

For the most common basis functions (impulse, pulse and triangle), $\overline{b}_l(\alpha)$ is

$$\overline{b}_l(\alpha) = \begin{cases} e^{j\alpha x_l} & : b_l(x) = \delta_l(x) \\ d_l \operatorname{sinc}\left(\frac{\alpha d_l}{2}\right) e^{j\alpha x_l} & : b_l(x) = p_l(x) \\ \frac{1}{j\alpha}\Big[e^{j\alpha(d_l^e)/2} \operatorname{sinc}\left(\alpha \frac{d_l^e}{2}\right) - e^{-j\alpha(d_l^b)/2} \operatorname{sinc}\left(\alpha \frac{d_l^b}{2}\right)\Big] e^{j\alpha x_l} & : b_l(x) = t_l(x). \end{cases} \quad \text{(A3)}$$

In the above $p_l(x)$ is a pulse function of unit height and width d_l, symmetrical about x_l; and $t_l(x)$ is a rooftop function having its maximum height (unity) at x_l and being zero for $x = x_l - d_l^b$ and $x = x_l + d_l^e$. There is no simple relationship between the $\overline{\rho}(\alpha|x_l)$ resulting from various basis functions (as exists for the direct MoM), because the Green's function is not translationally invariant. The A_{kl} elements are now given by

$$A_{kl} = \frac{1}{2\pi\epsilon_0(1+\epsilon_r)} \int_{-\infty}^{\infty} \overline{w}_k(\alpha) \frac{\tanh(\alpha b)}{\alpha} \overline{\rho}(\alpha|x_l) d\alpha, \quad \text{(A4)}$$

where the normalized testing functions $\overline{w}_k(\alpha)$ are

$$\overline{w}_k(\alpha) = \frac{\overline{b}_k(-\alpha)}{\overline{b}_k(0)} \quad \text{(A5)}$$

(note that for the triangle, $\overline{b}_k(0) = (d_k^b + d_k^e)/2$). This gives the A_{kl} elements for nine combinations of basis- and testing functions (note that in the case $b_l = \delta(x - x_l)$ and $w_k = \delta(x - x_k), x_l = x_k$ is not admissible).

Appendix B

This Appendix derives the charge induced on only *one* semi-infinite plate by a given charge density distribution (the plate occupies the half-plane $x < 0$). Defining

$$\overline{\phi}_+(\alpha) = \int_0^{\infty} \phi(x) e^{j\alpha x} dx, \quad \text{(B1)}$$

and

$$\overline{\rho}_-(\alpha) = \int_{-\infty}^{0} \rho(x, 0) e^{j\alpha x} dx, \quad \text{(B2)}$$

we get analogously to (5)

$$\overline{\rho}_-(\alpha) - \epsilon_0(1+\epsilon_r)\gamma \coth(\gamma b)\overline{\phi}_+(\alpha) = -\overline{b}_l(\alpha). \quad \text{(B3)}$$

Dividing (B3) by $\overline{K}_-(\alpha)$, applying the decomposition theorem and Liouville's theorem, and evaluating the occuring integrals by the residue theorem, we obtain the following equation for the charge distribution in the wavenumber domain

$$\overline{\rho}(\alpha|x_l) = \overline{b}_l(\alpha) + \overline{K}_-(\alpha) \sum_{n=1}^{\infty} p_n \frac{1}{(-\alpha + \alpha_n)} \overline{b}_l(\alpha_n). \quad \text{(B4)}$$

Using (B4) instead of (11) and (A2), (12) and (A3) to (A5) remain valid.

Acknowledgment

This work was made possible by Siemens Corporate Research, Munich. The authors express their thanks to Prof. F. J. Seifert, Prof. G. Magerl and Dr. C. Ruppel for their support and encouragement. The help of E. McMahon, B. van der Tannen, H. Reichinger, B. P. Oehry, and W. Schupita is gratefully acknowledged.

References

[1] N. Wiener and E. Hopf, "Über eine Klasse singulärer Integralgleichungen," *Sitzungsberichte der Preussischen Akademie der Wissenschaften* pp. 696–706, 1931.
[2] D. S. Jones, "A simplifying technique in the solution of a class of diffraction problems," *Quart. Jour. Math.*, vol. 3, pp. 189–196, 1952.
[3] B. Noble, *Methods Based on the Wiener-Hopf Technique.* London: Pergamon, 1958.
[4] R. Rojas, "Wiener-Hopf analysis of the EM diffraction by impedance discontinuity in a planar surface and by an impedance half-plane," *IEEE Trans. Antennas Propagat.*, vol. 36, pp. 71–83, 1988.
[5] S. Dowerah and A. Chakrabarti, "Extinction cross section of a dielectric strip," *IEEE Trans. Antennas Propagat.*, vol. 36, pp. 696–706, 1988.
[6] E. Lueneburg and R. A. Hurd, "Two waveguide bifurcation problems," *Z. Angew. Math. Mech.*, vol. 65, pp. 551–559, 1985.
[7] R. A. Hurd, "Diffraction by an anisotropic impedance half plane," *Can. J. Phys.*, vol. 63, pp. 1135–40, 1985.
[8] P. S. Deshwal, "Rayleigh wave scattering due to a surface impedance in a liquid layer," *J. Math. Phys. Sci.*, vol. 21, pp. 399–421, 1987.
[9] A. N. Zlatin and A. A. Khrapkov, "A semi-infinite crack parallel to the boundary of the elastic half-plane," *Sov. Phys. Dokl.*, vol. 31, pp. 810–813, 1986.
[10] R. Eaves and E. Bolle, "Modes on a shielded slot line," *Arch. El. Übertr.*, vol. 24, pp. 389–394, 1970.
[11] D. P. Morgan, *Surface Wave Devices for Signal Processing.* Amsterdam: Elsevier, 1985.
[12] B. Fleischmann, W. Ruile, G. Riha, and A. R. Baghai-Wadji, "Reproducable SAW filters at 2.5 GHz," *Int. Conf. on Frequency Control and Synthesis,* pp. 29–35, 1987.
[13] F. J. Seifert, G. Visintini, and C. Ruppel, "Diffraction compensation of SAW filters," in *Proc. 1990 IEEE Ultrason. Symp.*, pp. 67–76.
[14] R. F. Milsom, N. H. C. Reilly, and M. Redwood, "Analysis of generation and detection of surface and bulk acoustic waves by interdigital transducers," *IEEE Trans. Sonics Ultrason.*, vol. SU-24, pp. 147–167, 1977.
[15] A. R. Baghai-Wadji, O. Männer, and R. Ganß-Puchstein, "Analysis and measurement of transducer end radiation in SAW filters on strongly coupling substrates," *IEEE Trans. Microwave Theory Tech.*, vol. 37, pp. 150–158, 1989.
[16] R. F. Harrington: *Field Computation by Moment Method.* New York: Macmillan, 1968.
[17] R. Mittra and S. Lee, *Analytical Methods in the Theory of Guided Waves.* New York: Macmillan, 1973.
[18] A. F. Molisch, "On the application of the Wiener-Hopf-technique to the boundary-value-problems in electromagnetism," Diploma thesis, Technische Universität Wien, 1990, (in German).
[19] A. F. Molisch and A. R. Baghai-Wadji, "The electrostatic charge distribution on two semi-inifinite metallic plates induced by a line charge," in *Proc. 1990 4th IGTE-Symp.*, pp. 223–228.
[20] J. Meixner, "The behavior of electromagnetic fields at edges," *IEEE Trans. Antennas Propagat.*, vol. AP-20, pp. 442–446, 1972.
[21] P. M. Morse and H. Feshbach, *Methods of Theoretical Physics.* New York: McGraw-Hill, 1953.
[22] M. Abramowitz and I. A. Stegun, *Handbook of Mathematical Functions.* New York: Dover, 1970.
[23] R. C. Peach, "A general approach to the electrostatic problem of the SAW interdigital transducer," *IEEE Trans. Sonics Ultrason.*, vol. SU-28, pp. 96–105, 1981.
[24] F. Straker, *VLSICAP V1.3, User's Guide,* Institut für Allgemeine Elektrotechnik und Elektronik, Technische Universität Wien, Austria, 1986.
[25] O. Männer and R. Ganß-Puchstein, "Accurate computation of apodized SAW transducer capacitances," in *Proc. 1988 IEEE Ultrason. Symp.*, pp. 23–28.
[26] K. Bloetker, K. A. Ingebrigtsen, and H. Skeie, "Acoustic surface waves in piezoelectric materials with periodic metal strips on the surface," *IEEE Trans. Electron Devices,* vol. ED-20, pp. 1139–1146, 1973.

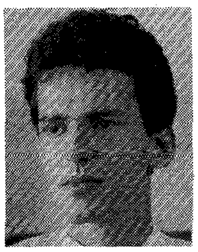

Andreas F. Molisch (S'89) was born in Vienna, Austria in 1966. He received the Dipl. Ing. degree (Hons.) from the Technical University of Vienna in Oct. 1990.

Since 1989, he has been a research assistant at the TU Vienna, first at the Department of Applied Electronics of the Institut für Allgemeine Elektrotechnik und Elektronik and since Feb. 1991, at the Institut für Nachrichtentechnik und Hochfrequenztechnik, where he is currently pursuing a doctoral degree. His research interests are electromagnetic boundary-value problems, quantum electronics, and radiative transfer.

Mr. Molisch was awarded the GiT-Förderungspreis of the Austrian Society of Electrical Engineering for his diploma thesis on the Wiener–Hopf method.

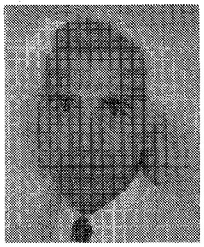

Ali R. Baghai-Wadji (M'88) was born in Marand, Iran, on May 6, 1953. He received Dipl. Ing. and Dr. Techn. degrees in electrical engineering from the Vienna University of Technology in 1984 and 1987, respectively.

In 1980 he joined the Institut für Allgemeine Elektrotechnik und Elektronik at Vienna University of Technology, where he was engaged in field analysis for surface acoustic wave devices. From 1984 to 1988 he was a Research Assistant at the Vienna University of Technology. Since 1988 he has been an Assistant Professor and the leader of the Wave Phenomena in Microelectronic Devices group at the same university. In July 1988 and July 1990, respectively, he was invited for one week stay at Polish Academy of Sciences in Warsaw and at Russian Academy of Sciences in Moscow. In 1989 he was elected a committee member of International Symposium on Surface Waves in Solids and Layered Structures. As a recipient of Kurt Gödel grant in 1990 and 1991, respectively, he spent three and four months at the University of California, Irvine, doing theoretical research on surface acoustic shape resonances.

Dr. Baghai-Wadji is the author of more than 40 publications in journals and conference proceedings. His areas of scientific interest include the development and application of numerical and anlaytical methods for the analysis of the radiation and scattering of piezoelectromagnetic waves. He is a member of Austrian Physical Society and German Physical Society.

Christian Schiebl received the Diplomingenieur degree in physics from the Technical University of Vienna in 1986. His master's thesis dealt with quantitative electron probe microanalysis (EPMA) using characteristic M-lines.

After graduation he joined the "Institut für Angewandte und Technische Physik" at the Technical University of Vienna where he received his doctor's degree in 1989. His dissertation was on fluorescence correction in quantitative EPMA. In 1989 he joined the Campus-based Engineering Center (CEC) in Vienna where he currently works in the field of semiconductor process and device simulation.